

function of oxygen transport during their typical lifespan of 120 d in the human body. Some medical devices such as synthetic heart valves can serve as additional mechanical challenges exacerbating fatigue damage and hemolysis of RBCs in circulation (8). Prior work has reported indirect measurement of deformation using shear flow of a population of cells in a microchannel (9) and observations of a reduction in deformability in RBC membranes as a result of static shear stresses (10, 11). However, systematic studies of mechanical fatigue at the single-cell level and experimental evidence for the occurrence of cyclic loading effects in biological cells have not been reported to date. Investigation of these issues is particularly significant because many of the models and mechanisms to characterize the mechanical properties of engineered materials, which are known to be severely susceptible to damage and failure by fatigue, are also widely adapted with appropriate modifications to describe the complex and clinically relevant mechanical behavior of biological cells in health and disease (12, 13).

There is thus a need for scientific investigations into mechanical fatigue to address the following fundamental questions:

First, what is the effect of fluctuations in stresses or deformation of a healthy biological cell on its mechanical and physical characteristics, structural integrity, and performance, as a function of such factors as the maximum intensity, amplitude and rate of strain, frequency of cyclic deformation, number of cycles, and so on?

Second, is the effect seen specific to cyclic variations in deformation? In other words, to what extent does it occur, by comparison, under static, quasi-static, or monotonic variations in deformation at comparable levels of maximum “intensity” of strain or stress for comparable durations of time?

In order to address these questions systematically, we choose the human RBC for the single-cell investigation. RBCs are highly specialized cells that are well adapted for respiratory gas exchange in the cardiovascular system. Their unique membrane structure, which comprises a lipid bilayer and a 2D cytoskeleton made of spectrin networks (14, 15), contributes to the intrinsic resilience of RBCs to withstand shear stresses induced by blood flow and repeated deformation exerted by physical constraints from capillaries and interendothelial slits (16). The absence of a nucleus and of a complex 3D cytoskeleton in the disk-shaped RBC further facilitates relatively easier analyses of cyclic deformation. In addition, as RBCs travel through blood vessels with variable vascular resistance (17) they are subjected to intermittent stresses and cyclic strains. During their lifespan, RBCs gradually lose their mechanical integrity (18), and senescent RBCs are eventually removed by splenic filtration (16). How the RBCs lose their mechanical integrity solely in response to cyclic deformation during their normal biological function is, therefore, a topic of considerable scientific and clinical interest. In certain infectious diseases (19, 20) and inherited blood disorders (21), survival of affected RBCs is remarkably reduced due to the abnormalities in cell membranes and the attendant changes in cell properties, and mechanical fatigue could contribute further to the loss of deformability of diseased cells.

In this work, we employed a unique and general experimental technique to investigate whether mechanical fatigue effects occur in biological cells and to address the foregoing fundamental questions that identify any possible role of mechanical fatigue in influencing the properties of RBCs. Our method employs amplitude-modulated electrodeformation in conjunction with microfluidics (22) (Fig. 1A) and is capable of imposing on the single RBCs controlled static loads for prolonged periods of time or large numbers of cyclically varying mechanical strains.

A sinusoidal carrier wave with a frequency of 1.58 MHz is selected for easy cell immobilization by positive dielectrophoresis (DEP) and electrodeformation (23). See *SI Appendix, Electro-Deformation Characterization of RBCs* for a summary of the principles underlying electrodeformation loading of RBCs and for details of experimental methods and sample preparation. *SI Appendix, Fig. S1A* graphically shows the rationale for the choice of a

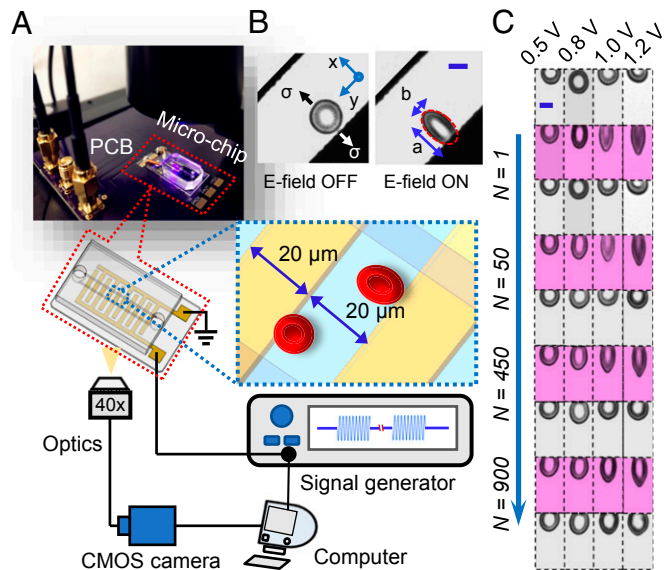


Fig. 1. Fatigue testing of single RBCs using amplitude-modulated electrodeformation. (A) Experimental setup for real-time measurement of cell deformation in a microfluidic chip. Schematic shows the key components of the testing system, including the microfluidic device with interdigitated microelectrodes, signal generator for producing modulated sinusoidal carrier wave, and computer for data acquisition, analysis, and modeling. (B) Microscopic images of a representative RBC when the electric field (E-field) is ON and OFF. Dimensions of RBC are measured along x and y axes (a and b , respectively). (C) Microscopic images of cell deformation at 4 representative loading levels arising from applied voltages of 0.5, 0.8, 1.0, and 1.2 V as functions of loading cycles ($N = 1, 50, 450$, and 900). (Scale bars in B and C, 5 μm .)

frequency of 1.58 MHz for the current experiments. *SI Appendix, Fig. S1 B–D* provide results of our parametric analysis of the effects of variations in cell membrane conductivity, cytoplasm permittivity, and cytoplasm conductivity, respectively, on the DEP response of RBCs. The freely suspended RBCs move toward the electrode edges by positive DEP and deform into a quasi-ellipsoid shape due to electrodeformation (Fig. 1B). Each RBC is individually tracked and analyzed.

Results

Morphological Characteristics of Fatigued RBCs. Cyclic tensile loading of constant amplitude was achieved by imposing a step-function voltage (rectangular waveform) to the carrier wave. The root-mean-square value of the voltage, which determines the peak load of the fatigue cycle, was fixed at 0.5, 0.8, 1.0, and 1.2 V. All of the voltage values reported in this paper refer to this root-mean-square voltage. Since the minimum voltage in the fully unloaded state is zero when the electrical input is fully turned off, the stress ratio or load ratio of the fatigue cycle, R , which is the ratio of the minimum to the maximum load (stress) of the fatigue cycle, is zero. A fixed time period of 4 s for cyclic loading and unloading, with 2 s for loading and 2 s for unloading, was used in the experiment (*Movie S1*). The cyclic loading frequency is thus 0.25 Hz with a rectangular waveform.

During the loading phase, cells rapidly deformed and attained an equilibrium between electrodeformation force and the resultant membrane elastic force in a finite period of time. This time period for deformation stabilized within 0.6 ± 0.2 s in the first fatigue cycle and it increased up to 1.5 ± 0.3 s after about 900 fatigue cycles, for all of the voltage levels. The RBCs gradually relaxed to their stress-free states during unloading, with the typical characteristic time for relaxation being 0.16 ± 0.04 s in the first cycle. Fig. 1C shows the time sequences of microscopic images of 4 representative

disk-shaped RBCs at the 4 voltages, for fatigue loading cycles $N = 1, 50, 450,$ and 900 . Regions highlighted in gray show cell shapes in the fully relaxed state and those in purple show the fully deformed state. Within the initial 50 cycles, cells were able to completely recover their initial disk shape upon unloading from the peak load. Permanent deformation in cell membranes started to occur only after about 450 fatigue cycles and continued for the remainder of cyclic loading. The extent of permanent deformation was higher at the higher voltages of 1.0 V and 1.2 V, as seen in Fig. 1C. Cell morphological change is quantified by the stretch ratio S_R , which is the ratio of the major axis, a , to the minor axis, b , of the cell fitted by an ellipse. Evolution of S_R values of 4 representative RBCs deformed by 0.5, 0.8, 1.0, and 1.2 V are plotted as functions of time, respectively (SI Appendix, Fig. S2 A–D). As seen in SI Appendix, Fig. S2, the time required for cells to attain a plateau in maximum S_R and the time for full relaxation extend significantly into many cycles of fatigue loading. These findings suggest that the deleterious effects of cyclic loads on RBC membrane damage are manifested only after a critical number of cycles and that they accumulate over hundreds of fatigue cycles. Permanent damage in cell membranes is consistently observed when the voltage level is in excess of 0.5 V. The characteristic features of fatigue damage in RBC membranes include pronounced shape changes from a disk shape into elliptocyte, stomatocyte, or knizocyte-like shapes, as well as the development of single to multiple thorny projections on cell membranes (SI Appendix, Fig. S2E).

Degradation in Mechanical Properties of RBCs. We characterized the mechanical properties of RBC membranes in response to different levels of shear stresses calibrated from different voltage values. Details of shear stress calibration can be found elsewhere (23). A brief description of our constitutive models for the viscoelastic deformation characteristics of RBCs and of the cell-membrane shear stresses is presented in SI Appendix, *Constitutive Model for Viscoelastic Deformation of RBC Membranes*. The applied voltage was kept at no more than 2.0 V to prevent any possible membrane damage that may occur outside of mechanical fatigue. For this reason, the loading was kept below certain threshold levels: a threshold electrical field strength of 2.1 kV/cm (24) and mechanical stress on the membrane of 150 Pa (25). For an assumed membrane thickness of 10 nm, the corresponding values of RBC membrane shear stresses were calculated to be 1.19 ± 0.22 Pa, 1.87 ± 0.42 Pa, 2.85 ± 0.77 Pa, 4.78 ± 1.48 Pa, and 9.63 ± 3.21 Pa for the applied voltages of 0.8, 1.0, 1.2, 1.5, and 2.0 V, respectively.

The dynamic deformation of RBCs is characterized by the transient value of the principal extension/contraction ratio, $\lambda(t)$, which is calculated by dividing the initial value of the minor axis, b_0 , by its transient value, $b(t)$.^{*} Fig. 2A shows the instantaneous value of λ as a function of number of fatigue cycles, N , for a particular

^{*}Note that $\lambda(t)$ is defined here in terms of the instantaneous value of the contraction ratio in the transverse direction of tensile cyclic loading, $b_0/b(t)$, rather than as the axial extension ratio, $a(t)/a_0$. This is because a small part of the deformed membrane along the tensile loading axis of axial dimension a is necessarily obstructed from view by the gold electrode when imaging the cell. This partial obstruction could lead to some error in the analysis of deformation if the latter definition of $\lambda(t)$ along the axial direction had been invoked. In SI Appendix, we demonstrate that the definition and choice of the instantaneous values of extension ratio based either on the axial extension ratio, $a(t)/a_0$, or the corresponding transverse contraction ratio, $b_0/b(t)$, has absolutely no effect on the trends discovered here about the role of mechanical fatigue in influencing the behavior of RBCs. There are, however, some anticipated differences in the quantitative values of key parameters characterizing mechanical fatigue effects between the 2 related definitions of actual values of $\lambda(t)$ because of the normal variations in cell response in this mutually orthogonal directions and the experimental scatter and errors in extracting axial and transverse dimensions during deformation from optical images. Because of the relatively greater accuracy of the former definition, $\lambda(t) = b_0/b(t)$, in the experimental measurements, all subsequent results on the principal extension ratio are presented in the paper, with this choice of definition. For completeness, we present all of the corresponding results obtained using the alternative definition of axial extension ratio, $a(t)/a_0$, in SI Appendix and demonstrate that none of the trends and conclusions reported here is unaffected by the particular choice of the definition of the extension ratio.

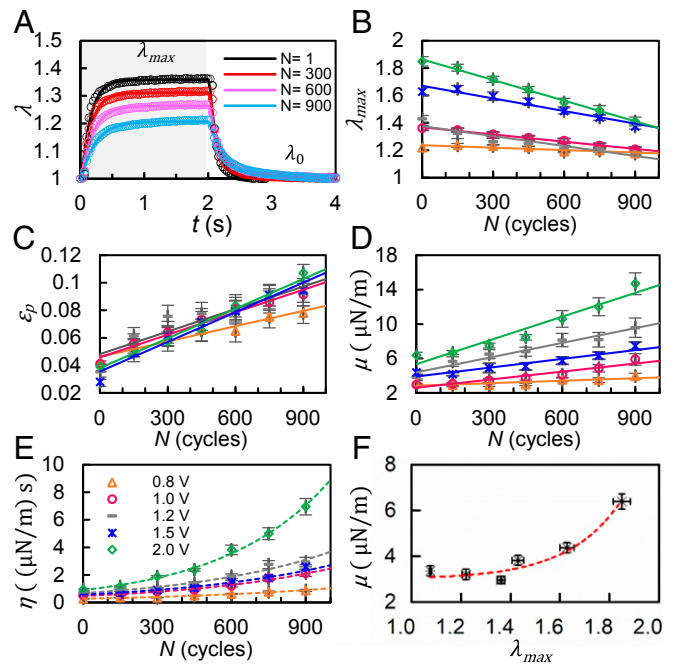


Fig. 2. Degradation of mechanical properties of RBCs under cyclic tensile loading of constant amplitude. (A) Instantaneous values of λ averaged from individually tracked cells ($n = 20$) in both stretching phase (gray region) and relaxation phase (white region) for $N = 1, 300, 600,$ and 900 fatigue cycles at 1.0 V. Open circles represent experimental measurement and the solid curves represent exponential fit to the data. (B–E) Variation of the mean value of λ_{\max} , ϵ_p , μ , and η , respectively, of RBCs with the number of fatigue loading cycles, N , for 5 different voltage levels of 0.8, 1.0, 1.2, 1.5, and 2.0 V (represented by the same set of symbols as shown in E). (F) Nonlinearity in membrane shear modulus, μ , plotted as a function of λ_{\max} at $N = 1$. The solid lines represent the best fit linear regression lines. The dashed lines represent the best fit exponential curves. Error bars indicate standard error of the mean (SEM).

voltage of 1.0 V. Values of λ during the stretching phase and the relaxation phase can be fitted well with an exponential function, $\lambda = A \times \exp(B \times t) + C$, for each cycle. We extract the maximum extension (λ_{\max}) and the minimum extension (λ_0) in the fully stretched and fully relaxed states, respectively. The initial value of λ_{\max} indicated by the vertical intercept ($\bar{\lambda}_{\max}$) increases with the voltage level as a result of higher resulting stresses, with the best-fit linear regression, $\bar{\lambda}_{\max} = 0.53 \times V + 0.82$, with $R^2 = 0.96$. Mean values of λ_{\max} decrease from 1.36 for $N = 1$ to 1.32, 1.27, and 1.21 for $N = 300, 600,$ and 900 , respectively.

The value of λ_{\max} strongly varies with the number of loading cycles for all stress levels. The best-fit linear regressions are $\lambda_{\max} = -8 \times 10^{-5} \times N + 1.25$ with $R^2 = 0.90$ for 0.8 V, $\lambda_{\max} = -2 \times 10^{-4} \times N + 1.37$, with $R^2 = 0.99$ for 1.0 V, $\lambda_{\max} = -2 \times 10^{-4} \times N + 1.38$, with $R^2 = 0.85$ for 1.2 V, $\lambda_{\max} = -3 \times 10^{-4} \times N + 1.67$, with $R^2 = 0.95$ for 1.5 V, and $\lambda_{\max} = -5 \times 10^{-4} \times N + 1.86$ with $R^2 = 1.0$ for 2.0 V, as shown in Fig. 2B. Additionally, the magnitude of the negative slope (m) of the lines decreases with increasing voltage, with the best-fit linear regression, $m = 3 \times 10^{-4} \times V - 2 \times 10^{-4}$, with $R^2 = 0.97$. These results indicate that the rate of mechanical damage of the cell membrane is proportional to the intensity of cyclic deformation which, in turn, depends on the magnitude of voltage.

In order to quantify and compare the extent of fatigue damage arising among the different cases, permanent deformation in RBC membrane during fatigue was evaluated by the effective plastic strain, $\epsilon_p = (S_{R_{\min}}(N) - 1/S_{R_{\min}}(N))/4$, where $S_{R_{\min}}$ denotes the minimum stretch ratio in fully relaxed state. The mean value of ϵ_p is proportional to the number of loading cycles ($R^2 > 0.9$; Fig. 2C). The slope of the linear functions increases with the voltage level,

suggesting that plastic strain accumulation occurs faster at higher voltage levels.

The viscoelastic characteristics of RBC membranes, including shear modulus and shear viscosity, vary significantly with the number of fatigue cycles (Fig. 2 D and E). For instance, at 1.2 V, the mean values of shear modulus increase from 3.82 $\mu\text{N/m}$ in the first fatigue cycle to 9.58 $\mu\text{N/m}$ for the 900th fatigue cycle. This is quantified with a linear regression analysis, $\mu = 5.7 \times 10^{-3} \times N + 4.4$ with $R^2 = 0.95$. In the first cycle, the shear modulus ranges from $3.2 \pm 0.2 \mu\text{N/m}$ at 0.8 V to $6.4 \pm 0.4 \mu\text{N/m}$ at 2.0 V. The nonlinear variation here of membrane shear modulus with the maximum extension ratio (Fig. 2F) is consistent with trends reported by previous studies for static deformation (26, 27). The mean value of membrane shear moduli measured at all voltage levels is $4.1 \pm 1.4 \mu\text{N/m}$, which is within the range of values in the literature, 1.8 to 11.3 $\mu\text{N/m}$, for healthy RBC membranes, from a number of independent studies that employ different experimental methods (28–30).

The membrane shear viscosity, η , was determined by multiplying the characteristic relaxation time, t_c , and the membrane shear elastic modulus, μ . The ensuing values, $\eta = 0.38$ to $0.88 \mu\text{N/m}\cdot\text{s}$, fall within the range of results reported from other independent experiments, 0.3 to 2.8 $\mu\text{N/m}\cdot\text{s}$ (29), for healthy RBCs. It is evident that both shear modulus and shear viscosity increase as a result of mechanical fatigue. The rate of fatigue-induced stiffening also increases with applied voltage. The shear viscosity increases from 0.72 $\mu\text{N/m}\cdot\text{s}$ at $N = 1$ to 2.93 $\mu\text{N/m}\cdot\text{s}$ at $N = 900$. This change can be represented by an exponential function $\eta = 0.68 \times \exp(1.7 \times 10^{-3} \times N)$ with $R^2 = 0.98$. Note that shear modulus and shear viscosity values measured after 900 cycles of fatigue loading at the highest load level of 2.0 V were as high as to 14.7 $\mu\text{N/m}$ and 6.95 $\mu\text{N/m}\cdot\text{s}$, respectively. These values are much higher than the corresponding upper-bound values reported for healthy, unfatigued (but statically or monotonically deformed) RBCs (29, 31). This trend again suggests that mechanical fatigue leads to alterations in structure and properties, including the stiffening of the cell membrane, of healthy RBCs that are distinctly different from those induced by static or monotonic loads.

Values of t_c are analyzed with an exponential fit to $\lambda(t)$ during the relaxation phase (such as that shown in the nonshaded region of Fig. 2A). SI Appendix, Fig. S3 shows the variation of t_c as a function of N , for 5 different voltage levels. For example, in the initial fatigue cycle for 1.0 V, $t_c = 0.16 \pm 0.04$ s, which is consistent with the values of 0.1 to 0.3 s reported in the literature on the basis of independent experimental techniques (31, 32). However, no correlation was found between t_c and the level of the applied voltages. After a sufficient number of cycles at 1.0 V, t_c increases to 0.17 ± 0.06 s, 0.21 ± 0.07 s, 0.22 ± 0.08 s, 0.28 ± 0.08 s, and 0.34 ± 0.10 s for $N = 150, 300, 450, 600,$ and 900 , respectively. Such progressive change in cellular relaxation behavior reflects the accumulation of viscous damage in RBC membranes as a result of mechanical fatigue.

In an attempt to quantify the stress dependence of fatigue damage in RBC membranes, we explore the conditions surrounding a 5% reduction in λ_{max} and define a critical number of fatigue cycles, N_s , required to achieve this level of change for different fatigue loading conditions. On the basis of this estimate, it is possible to develop a stress-life curve for the fatigue of RBCs, somewhat similar to the classical Wöhler curve in metal fatigue (1), which is shown in SI Appendix, Fig. S4.

Effect of Static Tensile Loading. In order to determine whether there exists a true mechanical fatigue effect in biological cells, we now consider static loading at a level of 1.2 V (Movie S2). The applied shear stress for this fixed load is estimated to be 2.85 Pa for the assumed membrane thickness of 10 nm. Fig. 3A shows the deformation response of 2 representative RBCs for which the

relative stretch ratio S_R is plotted as a function of time over which the voltage (load) is applied for 60 min. Each cell is stretched to a maximum S_R in a finite time and the initial elastic stretch from the sudden application of load persists for at least 10 min. Afterward, the S_R value decreases with time, indicating the stiffening process in RBC membranes due to the cumulative deleterious effect from sustained loading. This finding agrees with a previous study (33) that showed reduced deformability arising from sustained mechanical loads. Differences in the cellular behavior between these 2 cells likely arise from the normal heterogeneity in cell membranes. A small fraction of RBCs (30%) exhibited tank-treading motion after a certain period of time, which could be a manifestation of structural alteration in cell membranes as noted previously (34). This phenomenon is demonstrated by the time-dependent oscillations in S_R values after ~ 12 min in cell #2 (Fig. 3A and Movie S3). In order to quantify the progressive change in the mechanical properties in RBC membranes during static loading, the preset parameters μ , η , and ε_p have been obtained by a brief (20-s) deactivation of the static loading at every 10-min interval in a separate experiment but in parallel with the 60-min static loading. Fig. 3 B–D show the values of ε_p , μ , and η , respectively, averaged from 20 cells. Values of μ measured at $t = 20$ min are not significantly different from those measured at $t = 10$ min, while the values of η and ε_p are significantly higher ($P < 0.001$). All 3 parameters further increase during subsequent time intervals ($P < 0.001$). These results suggest, as anticipated, that static mechanical loading leads to changes in the characteristics of RBC membranes.

We develop additional quantitative comparisons of static deformation of RBCs with mechanical fatigue by contrasting the results for 2 different frequencies of constant-amplitude cyclic loading (rectangular waveform): 1) a time period of loading which occurs over 2 s, immediately followed by unloading lasting 2 s (i.e., a cyclic frequency of 0.25 Hz) for 2 applied voltages of 1.2 V and 2.0 V and 2) loading over 10 s, immediately followed by unloading lasting 10 s (i.e., a cyclic frequency of 0.05 Hz), also for the same 2 applied voltages of 1.2 V and 2.0 V. The deterioration in maximum deformation is quantified by the normalized relative extension

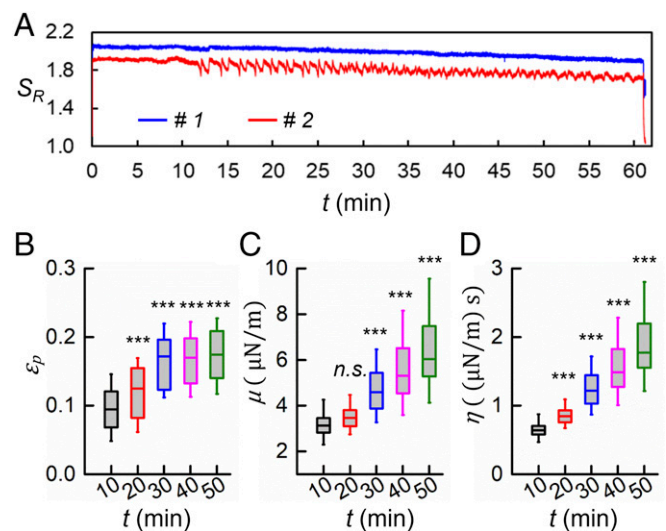


Fig. 3. Mechanical response of RBCs under static tensile loading. (A) Variation of relative stretch ratio as a function of time of 2 representative cells, #1 and #2, under the static loading at a constant voltage level of 1.2 V. (B–D) Values of ε_p , μ , and η of cells ($n = 20$) measured at 10, 20, 30, 40, and 50 min, respectively. *** $P < 0.001$; n.s., nonsignificant. Note the results here for static loading at the voltage of 1.2 V for 50 min correspond approximately to that obtained for cyclic loading with only 25 min of accumulated loading time at 1.2 V for 750 fatigue cycles (at a frequency of 0.25 Hz).

ratio, $\lambda_{\max}^* = \lambda_{\max} / \lambda_{\max, t=0}$. This represents the ratio of the instantaneous value of the relative extension ratio, λ_{\max} , of the RBC to that of the initial value of λ_{\max} at time $t = 0$. Fig. 4 shows the changes in λ_{\max}^* as a function of accumulated time under maximum load for static loading for the imposed voltages of 1.2 and 2 V in comparison to those under cyclic loading for the 2 frequencies with a rectangular waveform. This figure establishes that cyclic loading leads to a significantly greater reduction in the deformability of the cells than static loading. At the larger load, the lower-frequency cyclic loading (longer loading time) shows a relatively smaller loss in deformability (and a trend closer to that of the static loading case). The relative loss of deformability of RBCs under cyclic loading was as much as $11.9 \pm 0.01\%$ for 1.2 V and $21.7 \pm 0.02\%$ for 2 V, compared to the static loading case. The actual variation of λ_{\max} as a function of time is shown in *SI Appendix, Fig. S5*.

Effect of Loading Waveform on Mechanical Fatigue. As strain rate is an important variable, along with strain, for the characterization of viscoelastic behavior of cell membranes (35, 36), we examined the effect of waveform (for a fixed cyclic loading frequency of 0.25 Hz). For this purpose, we compared mechanical fatigue with a rectangular waveform to that with a half-wave rectified (HWR) sinusoidal waveform. This latter waveform was achieved by modulating the amplitude of the 1.58-MHz carrier wave, $V = 1.2\sin(\pi t/2)$, with the period of 4 s, which comprised a 2-s duration of loading time (*SI Appendix, Fig. S6A* and *Movie S4*) and an equal time for unloading (with the voltage turned off) and relaxation. *SI Appendix, Fig. S6B* shows the instantaneous S_R values of RBC membranes, averaged from 22 measurements, as a function of time at fatigue loading cycles, $N = 1, 300, 450, 600,$ and 900 . We observed that cell membranes gradually deformed to a maximum S_R and then gradually relaxed to a minimum during each cycle. The 2-s relaxation interval was sufficient for deformed cell membranes to fully recover their shape before the next loading cycle.

Similar to the fatigue characteristics of cell membranes under rectangular-waveform cyclic loading, the maximum S_R values for the sinusoidal loading was found to decrease with the number of loading cycles while the minimum S_R increased along with the loading cycles (*SI Appendix, Fig. S6B*). The peaks of the S_R shifted and showed a greater hysteresis of membrane cyclic deformation with increasing fatigue cycles (marked by the dashed line in *SI*

Appendix, Fig. S6A). The lag between the peak stress and peak deformation S_R increased approximately from 0 s at $N = 1$ to 0.13 s at $N = 900$, indicating an increase in viscosity of the cell membrane. To quantify the membrane viscosity, the characteristic time t_c was determined from the relaxation process when the external force was removed, using *SI Appendix, Eq. 9* similarly to that used to obtain *SI Appendix, Fig. S3*. A significant rise in t_c was noticed, from 0.16 s to 0.43 s in ~ 900 loading cycles.

Fig. 5A shows the stress-strain (σ - ϵ) hysteresis loops of cell membranes. The maximum shear strain decreased gradually from 0.96 at $N = 1$ to 0.84, 0.74, 0.59, and 0.53 at $N = 300, 450, 600,$ and 900 , respectively. More importantly, we observed appreciable progressive change in the dissipated hysteresis energy E , determined from the enclosed area of the fatigue hysteresis loop. During the initial 300 loading cycles, the value of E remained approximately constant at 0.20 to 0.21 $\mu\text{J}/\text{m}^2$ and then gradually increased to 0.31 $\mu\text{J}/\text{m}^2$ for $N = 450$ before attaining a plateau value of $\sim 0.40 \mu\text{J}/\text{m}^2$ between $N = 600$ and $N = 900$. Correlation between the dissipated energy E and the number of loading cycles was strong with $R^2 = 0.99$, with the best-fit Boltzmann growth line given by the expression $E = 0.4 / 0.2 / (1 + \exp((N - 445)/50)) \mu\text{J}/\text{m}^2$. The total dissipated energy up to the inflection point ($N = 445$ cycles) was estimated to be 96 $\mu\text{J}/\text{m}^2$, which is on the order of the energy, 80 $\mu\text{J}/\text{m}^2$, required for dissociation between the phospholipid bilayer of the RBC membrane and its cytoskeletal comprising the spectrin network (15). The values of $\epsilon_p, \mu,$ and η for the HWR sinusoidal waveform loading were compared to those for the rectangular waveform loading (Fig. 5 B-D). The membrane shear modulus is higher in the case of rectangular waveform loading than that for the sinusoidal amplitude loading. Here, the shear modulus for the former became significantly higher after 300 loading cycles ($P < 0.001$). However, η is not significantly different between the 2 different waveforms ($P > 0.05$ after 900 cycles). Furthermore, the evolution of permanent deformation, ϵ_p , in cell membranes was significantly faster for the rectangular waveform than for the sinusoidal waveform ($P < 0.05$ after 300 cycles).

Discussion and Concluding Remarks

In this work, we demonstrated a mechanical fatigue testing method for biological cells, using a microfluidics-based, amplitude-modulated, electrodeformation technique. The fatigue testing platform features multiple and unique advantages for the quantitative characterization of fatigue of single biological cells. The strengths of the method lie in its simplicity and flexibility to impose controlled mechanical loads (through positive DEP) at selected frequencies and waveforms, and its capability to probe a number of single cells over thousands of fatigue cycles. In this paper, we have presented results here that quantitatively establish the following results and mechanistic insights:

- 1) Repeated cyclic loading of healthy human RBCs under well-controlled loads, cyclic frequency, and waveform leads to an intrinsic mechanical fatigue effect in the biological cell. Our experimental method provides a unique means of quantifying cyclic deformation characteristics along and transverse to the loading direction (in *SI Appendix, Figs. S8 and S9* and here in the main text) and their implications for the properties and performance of RBCs.
- 2) Mechanical fatigue of RBCs leads to a much more pronounced effect on the physical properties such as deformability, membrane shear modulus, and membrane viscosity than static loading of the same maximum voltage or load imposed on the cell for the same accumulated loading time.
- 3) Mechanical fatigue leads to hysteresis and energy dissipation of a magnitude that could be sufficient to cause dissociation of the cell membrane from its cytoskeleton, and that permanent strains progressively accumulate with fatigue cycling. These results illustrate how continued mechanical fatigue can be detrimental to the structural integrity, and hence the biological function, of the RBC, beyond the damage induced by static loads.

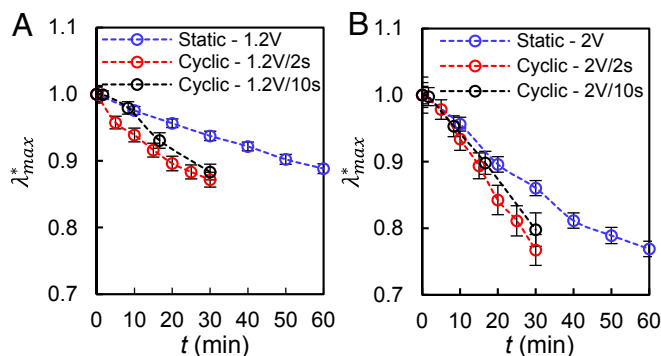


Fig. 4. Reduction of maximum relative deformation of RBCs as a function of accumulated loading time under static loading and cyclic loading with a rectangular waveform: Normalized λ_{\max}^* of healthy cells under (A) 1.2 V static loading ($n = 35$, blue circles), 1.2 V–2 s cyclic loading ($n = 58$, red circles), and 1.2 V–10 s cyclic loading ($n = 49$, black circles) and (B) 2.0 V static loading ($n = 27$, blue circles), 2.0–2 s cyclic loading ($n = 20$, red circles), and 2.0 V–10 s cyclic loading ($n = 40$, black circles). Error bars indicate SEM. Similar results comparing maximum extension ratio along the axial direction of loading between static and cyclic loading cases are given in *SI Appendix*.

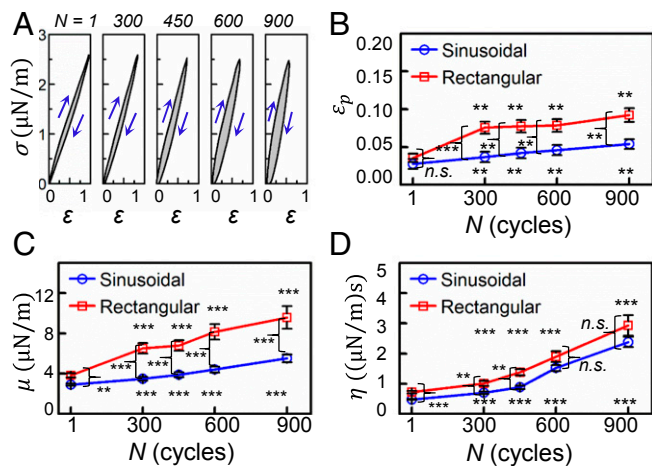


Fig. 5. Effect of loading waveform on mechanical degradation of RBCs during constant-amplitude mechanical fatigue. (A) Stress-strain curves showing the hysteresis loops (shaded region enclosed by the loading and unloading curves) for the indicated number of fatigue cycles for the HWR sinusoidal waveform. Blue arrows indicate loading and unloading in each case. (B–D) Variation of ϵ_p , μ , and η as a function of the number of fatigue cycles, and comparisons of mechanical characteristics between the HWR sinusoidal loading and the rectangular step-function waveforms for the indicated fatigue cycles. Error bars indicate SEM. ****** $P < 0.01$, ******* $P < 0.001$; n.s., nonsignificant.

4) The values of membrane shear modulus, viscosity, and the characteristic time of relaxation extracted from our experiments at the commencement of fatigue loading are in the range of values reported in the literature for healthy, unfatigued RBCs, using a variety of independent experimental methods. We show systematically that with the progression of mechanical fatigue the membrane shear modulus increases, approaching values that are comparable to pathological RBCs structurally altered by disease states. For example, the increase in membrane shear modulus of the healthy RBC to about $15 \mu\text{N/m}$ solely as a result of mechanical fatigue within 1,000 fatigue cycles is roughly comparable in magnitude to the increase in membrane shear modulus of a ring-stage RBC after it is invaded by a *Plasmodium falciparum* malaria parasite (20, 27).

The conditions of fatigue loading in our *in vitro* microfluidic assay are constrained by the need to allow cells to fully relax from the deformed state after each fatigue cycle prior to the imposition of the next cycle. This somewhat limited the choice of the loading frequency. To ascertain that the cells were viable through the entire duration of the mechanical fatigue tests, we conducted a series of separate experiments to determine the viability of RBCs after 1 h of cyclic loading at 1.2 V at a frequency of 0.25 Hz with rectangular waveform. Standard cell viability assays (for details see *SI Appendix, RBC Viability Assay*) reveal that about 98% of the cells are still viable after mechanical fatigue testing.

Additional considerations of how the current *in vitro* results of mechanical fatigue connect to the much more complex *in vivo* conditions of cyclic straining are provided herein. The maximum (absolute) tensile strain within the RBC membrane (spectrin network) while the RBCs traverse the smallest capillaries was estimated to be on the order of 50% (corresponding to a local spectrin network stretch ratio of 1.7) (37). Note that these maximum tensile strain values are comparable to the average tensile strains obtained by optical tweezers experiments of healthy RBCs stretched uniaxially under a tensile force of 67 to 130 pN (38, 39). The extent of deformation induced by the electric field on the RBCs in our work is also comparable to the mechanical deformation imposed by optical tweezers under equivalent stretching forces (40). When RBCs circulate in larger blood

vessels, they experience much less distortion and deformation. Considering that the maximum strain due to bending and total bending energy are both relatively much smaller compared to the in-plane strains and related strain energy due to stretch or shear [in most cases influences from bending are negligible compared to stretch (41, 42)], we take the zero strain as the minimum RBC membrane strain during blood circulation.

Considering that the lung-to-lung circulation time of blood in healthy subjects is about 55 s (43), and that the average lifespan of a healthy RBC in the human body is about 120 d, we can estimate the total number of fatigue cycles that an RBC is subjected to is about 1.9×10^5 . This estimate of *in vivo* fatigue cycles is about 200 times greater than the maximum number of fatigue cycles of about 900 considered in our *in vitro* system, during the course of which significant fatigue damage is found to occur.

Such a comparison then raises the following question: How do RBCs perform their biological function of gas transport *in vivo* without being affected by the effects of mechanical fatigue that can occur in as few as 900 cycles (i.e., about 0.5% of their lifespan)? This apparent paradox is rationalized on the basis of the following considerations. First, the maximum DEP electric field in our experiments would load RBCs in such a way that it produces an average tensile strain similar to the maximum local strains RBCs experience when traversing the smallest capillaries. In other words, our testing conditions simulate beyond the most stringent mechanical constraint conditions *in vivo* that lead to the maximum local strains, and they do not simulate the typical average cyclic strain on the RBCs during their lifespan. In addition, in our experiments the RBCs are quickly shuffled between the 2 extreme situations (maximum tension and zero strain), while *in vivo* the RBCs take an average of about 55 s between the maximum mechanical challenge and many partially unloaded intermediate configurations. Second, there are many additional factors that contribute to the fatigue life of RBCs, including the type of deformation, stress/strain amplitudes, cyclic frequency, loading rate, cytoadherence between their external surfaces and the endothelial cells lining the blood vessels, and so on. These effects representing complex *in vivo* conditions are not fully captured in the *in vitro* experiments. Third, in our experiments we find that RBCs do not lyse even after 900 cycles simulating severe deformation conditions. It is likely that significantly greater numbers of mechanical fatigue are needed to lyse the RBCs.

As in our *in vitro* testing, RBCs are subjected to rigorously modulated loading conditions, including static and cyclic deformation at various stress levels. Our method thus provides an accelerated test for assessing fatigue failure in RBC membranes due to mechanical loading.

On the other hand, as assessed by the viability assay of RBCs subjected to 1 h (900 cycles) of loading, the viability of RBCs is very high, at $98 \pm 2\%$ (see the discussion on RBC viability in *SI Appendix, RBC Viability Assay*). Therefore, it is likely that the electric field does not contribute significantly to the difference between the *in vivo* and *in vitro* observations.

The system developed here is also amenable to conducting mechanical fatigue experiments in conjunction with cellular gaseous microenvironments (44, 45) to create realistic, multifaceted loading scenarios to relate *in vitro* fatigue characteristics to the *in vivo* behavior of RBCs subjected to repeated straining during blood circulation. A recently developed hypoxia assay for the study of sickle cell disease (45, 46) in a microfluidic system can be integrated into the current fatigue testing platform to measure the mechanical strength and residual life span of circulating RBCs in more physiologically appropriate conditions.

Methods

Experimental Setup. The microfluidic chips for the fatigue test were made using a polydimethylsiloxane channel with 2 interdigitated electrodes coated on glass. More details are given in *SI Appendix, Experimental Setup*.

Sample Preparation. Blood samples from healthy donors were obtained with institutional review board approval from Florida Atlantic University. All blood

samples used were deidentified prior to use in the study. More details are given in *SI Appendix, Sample Preparation*.

ACKNOWLEDGMENTS. This work was supported by National Science Foundation Grants 1635312 and 1464102. M.D. acknowledges support from NIH Grant U01HL114476. S.S. acknowledges Nanyang Technological University, Singapore, for support through the Distinguished University Professorship.

1. S. Suresh, *Fatigue of Materials* (Cambridge University Press, Cambridge, UK, ed. 2, 1998).
2. International ASTM, *Fatigue Standards and Fracture Standards* (International ASTM, West Conshohocken, PA, 2018).
3. L. B. Freund, S. Suresh, *Thin Film Materials: Stress, Defect Formation and Surface Evolution* (Cambridge University Press, Cambridge, UK, 2004).
4. J. J. Kruzic, R. O. Ritchie, Fatigue of mineralized tissues: Cortical bone and dentin. *J. Mech. Behav. Biomed. Mater.* **1**, 3–17 (2008).
5. K. Shemtov-Yona, D. Rittel, Fatigue of dental implants: Facts and fallacies. *Dent J (Basel)* **4**, E16 (2016).
6. R. H. Dauskardt, R. O. Ritchie, J. K. Takemoto, A. M. Brendzel, Cyclic fatigue and fracture in pyrolytic carbon-coated graphite mechanical heart-valve prostheses: Role of small cracks in life prediction. *J. Biomed. Mater. Res.* **28**, 791–804 (1994).
7. R. Bai, J. Yang, Z. Suo, Fatigue of hydrogels. *Eur. J. Mech. A Solid.* **74**, 337–370 (2019).
8. L. Musumeci *et al.*, Prosthetic aortic valves: Challenges and solutions. *Front. Cardiovasc. Med.* **5**, 46 (2018).
9. S. Sakuma *et al.*, Red blood cell fatigue evaluation based on the close-encountering point between extensibility and recoverability. *Lab Chip* **14**, 1135–1141 (2014).
10. M. J. Simmonds, H. J. Meiselman, Prediction of the level and duration of shear stress exposure that induces subhemolytic damage to erythrocytes. *Biorheology* **53**, 237–249 (2016).
11. T. Mizuno *et al.*, Ultrastructural alterations in red blood cell membranes exposed to shear stress. *ASAIO J.* **48**, 668–670 (2002).
12. G. Bao, S. Suresh, Cell and molecular mechanics of biological materials. *Nat. Mater.* **2**, 715–725 (2003).
13. S. Suresh, Biomechanics and biophysics of cancer cells. *Acta Biomater.* **3**, 413–438 (2007).
14. J.-B. Fournier, D. Lacoste, E. Raphaël, Fluctuation spectrum of fluid membranes coupled to an elastic meshwork: Jump of the effective surface tension at the mesh size. *Phys. Rev. Lett.* **92**, 018102 (2004).
15. Z. Peng *et al.*, Lipid bilayer and cytoskeletal interactions in a red blood cell. *Proc. Natl. Acad. Sci. U.S.A.* **110**, 13356–13361 (2013).
16. I. V. Pivkin *et al.*, Biomechanics of red blood cells in human spleen and consequences for physiology and disease. *Proc. Natl. Acad. Sci. U.S.A.* **113**, 7804–7809 (2016).
17. C. E. Riva, J. E. Grunwald, S. H. Sinclair, B. L. Petrig, Blood velocity and volumetric flow rate in human retinal vessels. *Invest. Ophthalmol. Vis. Sci.* **26**, 1124–1132 (1985).
18. F. Lang, E. Lang, M. Föllner, Physiology and pathophysiology of eryptosis. *Transfus. Med. Hemother.* **39**, 308–314 (2012).
19. A. M. Dondorp, P. A. Kager, J. Vreeken, N. J. White, Abnormal blood flow and red blood cell deformability in severe malaria. *Parasitol. Today* **16**, 228–232 (2000).
20. S. Suresh *et al.*, Connections between single-cell biomechanics and human disease states: Gastrointestinal cancer and malaria. *Acta Biomater.* **1**, 15–30 (2005).
21. J. Narla, N. Mohandas, Red cell membrane disorders. *Int. J. Lab. Hematol.* **39** (suppl. 1), 47–52 (2017).
22. Y. Qiang, J. Liu, E. Du, Dynamic fatigue measurement of human erythrocytes using dielectrophoresis. *Acta Biomater.* **57**, 352–362 (2017).
23. Y. Qiang, J. Liu, F. Yang, D. Dieujeste, E. Du, Modeling erythrocyte electro-deformation in response to amplitude modulated electric waveforms. *Sci. Rep.* **8**, 10224 (2018).
24. E. H. Serpersu, K. Kinosita, Jr, T. Y. Tsong, Reversible and irreversible modification of erythrocyte membrane permeability by electric field. *Biochim. Biophys. Acta* **812**, 779–785 (1985).
25. L. B. Leverett, J. D. Hellums, C. P. Alfrey, E. C. Lynch, Red blood cell damage by shear stress. *Biophys. J.* **12**, 257–273 (1972).
26. Y. Qiang, J. Liu, E. Du, Dielectrophoresis testing of nonlinear viscoelastic behaviors of human red blood cells. *Micromachines (Basel)* **9**, 21 (2018).
27. J. P. Mills *et al.*, Effect of plasmodial RESA protein on deformability of human red blood cells harboring *Plasmodium falciparum*. *Proc. Natl. Acad. Sci. U.S.A.* **104**, 9213–9217 (2007).
28. H. Zhang, K.-K. Liu, Optical tweezers for single cells. *J. R. Soc. Interface* **5**, 671–690 (2008).
29. R. M. Hochmuth, R. E. Waugh, Erythrocyte membrane elasticity and viscosity. *Annu. Rev. Physiol.* **49**, 209–219 (1987).
30. M. M. Haque, M. G. Moisescu, S. Valkai, A. Dér, T. Savopol, Stretching of red blood cells using an electro-optics trap. *Biomed. Opt. Express* **6**, 118–123 (2014).
31. S. Chien, K. L. Sung, R. Skalak, S. Usami, A. Tözeren, Theoretical and experimental studies on viscoelastic properties of erythrocyte membrane. *Biophys. J.* **24**, 463–487 (1978).
32. R. M. Hochmuth, P. R. Worthy, E. A. Evans, Red cell extensional recovery and the determination of membrane viscosity. *Biophys. J.* **26**, 101–114 (1979).
33. M. Horade, C.-H. D. Tsai, H. Ito, M. Kaneko, Red blood cell responses during a long-standing load in a microfluidic constriction. *Micromachines* **8**, 100 (2017).
34. T. M. Fischer, M. Stöhr-Lissen, H. Schmid-Schönbein, The red cell as a fluid droplet: Tank tread-like motion of the human erythrocyte membrane in shear flow. *Science* **202**, 894–896 (1978).
35. Y.-Z. Yoon, J. Kotar, G. Yoon, P. Cicuta, The nonlinear mechanical response of the red blood cell. *Phys. Biol.* **5**, 036007 (2008).
36. J. Mancuso, W. Ristenpart, Stretching of red blood cells at high strain rates. *Phys. Rev. Fluids* **2**, 101101 (2017).
37. D. J. Quinn *et al.*, Combined simulation and experimental study of large deformation of red blood cells in microfluidic systems. *Ann. Biomed. Eng.* **39**, 1041–1050 (2011).
38. M. Dao, C. T. Lim, S. Suresh, Mechanics of the human red blood cell deformed by optical tweezers. *J. Mech. Phys. Solids* **51**, 2259–2280 (2003).
39. J. P. Mills, L. Qie, M. Dao, C. T. Lim, S. Suresh, Nonlinear elastic and viscoelastic deformation of the human red blood cell with optical tweezers. *Mech. Chem. Biosyst.* **1**, 169–180 (2004).
40. E. Du, M. Dao, S. Suresh, Quantitative biomechanics of healthy and diseased human red blood cells using dielectrophoresis in a microfluidic system. *Extreme Mech. Lett.* **1**, 35–41 (2014).
41. Y. C. Fung, P. Tong, Theory of the spherizing of red blood cells. *Biophys. J.* **8**, 175–198 (1968).
42. R. Skalak, A. Tozeren, R. P. Zarda, S. Chien, Strain energy function of red blood cell membranes. *Biophys. J.* **13**, 245–264 (1973).
43. N. R. Morris, E. M. Snyder, K. C. Beck, B. D. Johnson, Lung-to-lung circulation times during exercise in heart failure. *Eur. J. Appl. Physiol.* **106**, 621–627 (2009).
44. F. Padilla, P. A. Bromberg, W. N. Jensen, The sickle-unsickle cycle: A cause of cell fragmentation leading to permanently deformed cells. *Blood* **41**, 653–660 (1973).
45. E. Du, M. Diez-Silva, G. J. Kato, M. Dao, S. Suresh, Kinetics of sickle cell bioreology and implications for painful vasoocclusive crisis. *Proc. Natl. Acad. Sci. U.S.A.* **112**, 1422–1427 (2015).
46. E. Du, M. Dao, Faster sickling kinetics and sickle cell shape evolution during repeated deoxygenation and oxygenation cycles. *Exp. Mech.* **59**, 319–325 (2019).